



NONLINEAR ANALYSIS OF ANISOTROPIC PLATES WITH INITIAL IMPERFECTIONS AND VARIOUS BOUNDARY CONDITIONS SUBJECTED TO COMBINED BIAXIAL COMPRESSION AND SHEAR LOADS

GIULIO ROMEO and GIACOMO FRULLA

Politecnico di Torino, Department of Aerospace Engineering, C.so Duca degli Abruzzi 24, 10129 Turin, Italy

(Received 11 March 1993; in revised form 24 September 1993)

Abstract—The postbuckling behaviour of anisotropic panels with initial imperfections is investigated. Nonlinear analysis is developed for symmetric panels under combined biaxial compression and shear loads in order to obtain the out-of-plane panel deflection in the postbuckling range. The nonlinear differential equations are obtained by using the principle of the stationary value of the total potential energy and are expressed in terms of the out-of-plane displacement and the Airy function. They are solved with the Galerkin method for various boundary conditions. The theoretical results are in good agreement with the few results concerning isotropic plates and the simply supported anisotropic results found in literature. A new and original test facility was built in order to apply simultaneously both biaxial compression and shear loads. An anisotropic panel, clamped along the four edges, has been tested under different combined loads; the correlation between the experimental and analytical results has been quite good. The results demonstrate the influence of initial imperfections on panel deflection in the postbuckling range: the curves obtained experimentally in the presence of imperfections cross those obtained theoretically, where imperfections are ignored (producing lower out-of-plane deflection).

1. INTRODUCTION

While metallic panels are usually designed to work in the postbuckling field, panels made of composite materials are not permitted to exceed the buckling load. However, several analytical (Stein, 1985) and experimental results (Starnes and Rouse, 1981; Starnes *et al.*, 1984; Rouse, 1985) have shown a noticeable postbuckling behaviour of the composite panels before failure occurs, depending on the width-to-thickness ratio. An analytical solution is presented in this paper to investigate the postbuckling behaviour of simply supported and/or fully clamped anisotropic plates under combined biaxial compression and shear load. Since panels are often not perfectly manufactured, initial imperfections are also included in the analysis; such imperfections, in fact, considerably influence the out-of-plane displacement behaviour of the panel and cannot be ignored. No analytical and experimental results were found in open literature on such loading and boundary conditions. On the basis of these considerations, a new test facility was built at the Polytechnic of Turin in order to apply simultaneously both biaxial compression and shear loads (Romeo and Frulla, 1992).

2. THEORETICAL ANALYSIS

The classical laminate theory has to be modified for the postbuckling analysis of anisotropic plates under combined biaxial compression and shear loads. In fact, the strain–displacement relations become nonlinear when the components due to the out-of-plane deflection are taken into account. Plates with the initial imperfections w_0 have been studied on the basis of the Marguerre approximate nonlinear theory (Chia, 1980). The resultant strain–displacement relations are:

$$\begin{aligned}
\varepsilon_x &= u_{,x} + \frac{1}{2}w_{,x}^2 + w_{0,x}w_{,x} - zw_{,xx} \\
\varepsilon_y &= v_{,y} + \frac{1}{2}w_{,y}^2 + w_{0,y}w_{,y} - zw_{,yy} \\
\varepsilon_{xy} &= u_{,y} + v_{,x} + w_{,x}w_{,y} + w_{0,y}w_{,x} + w_{0,x}w_{,y} - 2zw_{,xy}
\end{aligned} \quad (1)$$

Where u, v, w are the displacement components of the middle surface and $\varepsilon_x, \varepsilon_y, \varepsilon_{xy}$ are the panel strain components. An index separated by a comma represents a derivative. By using the principle of the stationary value of the total potential energy, the equilibrium equations are worked out:

$$\begin{aligned}
N_{x,x} + N_{xy,y} &= 0 \\
N_{y,y} + N_{xy,x} &= 0 \\
M_{x,xx} + M_{y,yy} + 2M_{xy,xy} + N_x w_{,xx} + N_y w_{,yy} + 2N_{xy} w_{,xy} + N_x w_{0,xx} + N_y w_{0,yy} + 2N_{xy} w_{0,xy} &= 0,
\end{aligned} \quad (2)$$

in which $N_x, N_y, N_{xy}, M_x, M_y, M_{xy}$ represent forces and moment per unit length, respectively. By introducing the Airy function $\psi(x, y)$ as:

$$N_x = \psi_{,yy}, \quad N_y = \psi_{,xx}, \quad N_{xy} = -\psi_{,xy}, \quad (3)$$

the first two equilibrium equations are identically satisfied and the third equation becomes:

$$M_{x,xx} + M_{y,yy} + 2M_{xy,xy} + \psi_{,yy} w_{,xx} + \psi_{,xx} w_{,yy} - 2\psi_{,xy} w_{,xy} + \psi_{,yy} w_{0,xx} + \psi_{,xx} w_{0,yy} - 2\psi_{,xy} w_{0,xy} = 0. \quad (4)$$

The compatibility equation is introduced, in conjunction with eqn (4), for panels with initial imperfections as:

$$\varepsilon_{x,yy}^0 + \varepsilon_{y,xx}^0 - \varepsilon_{xy,xy}^0 = w_{,xy}^2 - w_{,xx} w_{,yy} + 2w_{0,xy} w_{,xy} - w_{0,yy} w_{,xx} - w_{0,xx} w_{,yy}, \quad (5)$$

where $\varepsilon_x^0, \varepsilon_y^0, \varepsilon_{xy}^0$ are the strain components of the middle surface. The stress-strain relations in terms of the ψ function and the out-of-plane displacement for symmetric panel, are:

$$\{\varepsilon_x^0, \varepsilon_y^0, \varepsilon_{xy}^0\}^T = [A^{-1}] \{\psi_{,yy}, \psi_{,xx}, -\psi_{,xy}\}^T \quad (6)$$

$$\{M_x, M_y, M_{xy}\}^T = [D] \{-w_{,xx}, -w_{,yy}, -2w_{,xy}\}^T, \quad (7)$$

in which $[A]$ and $[D]$ are the extensional and the bending stiffness matrices, respectively. By substituting the stress-strain relations in eqns (4) and (5) and normalizing as (Zhang and Mathews, 1984, 1985):

$$\begin{aligned}
\xi = x/a \quad \eta = y/b \quad \zeta = z/h \quad \lambda = a/b \quad F = \psi/A_{22}h^2 \quad T = W_0 = w_0/h \\
[A^*] = [A^{-1}] \quad [\bar{A}^*] = A_{22}[A^*] \quad W = w/h \quad [D^*] = [D] \quad [\bar{D}^*] = \frac{1}{h^2 A_{22}} [D^*],
\end{aligned} \quad (8)$$

the following governing system is obtained:

$$\begin{aligned}
\bar{D}_{11}^* W_{,\xi\xi\xi\xi} + 4\bar{D}_{16}^* \lambda W_{,\xi\xi\xi\eta} + 2(\bar{D}_{12}^* + 2\bar{D}_{66}^*) \lambda^2 W_{,\xi\xi\eta\eta} + 4\bar{D}_{26}^* \lambda^3 W_{,\xi\eta\eta\eta} + \bar{D}_{22}^* \lambda^4 W_{,\eta\eta\eta\eta} \\
- \lambda^2 (F_{,\eta\eta} W_{,\xi\xi} + F_{,\xi\xi} W_{,\eta\eta} - 2F_{,\xi\eta} W_{,\xi\eta} + F_{,\eta\eta} W_{0,\xi\xi} + F_{,\xi\xi} W_{0,\eta\eta} - 2F_{,\xi\eta} W_{0,\xi\eta}) = 0
\end{aligned} \quad (9)$$

$$\begin{aligned}
\bar{A}_{11}^* \lambda^4 F_{,\eta\eta\eta\eta} - 2\bar{A}_{16}^* \lambda^3 F_{,\xi\eta\eta\eta} + (2\bar{A}_{12}^* + \bar{A}_{66}^*) \lambda^2 F_{,\xi\xi\eta\eta} - 2\bar{A}_{26}^* \lambda F_{,\xi\xi\xi\eta} + \bar{A}_{22}^* F_{,\xi\xi\xi\xi} \\
= \lambda^2 (W_{,\xi\eta}^2 - W_{,\xi\xi} W_{,\eta\eta} + 2W_{0,\xi\eta} W_{,\xi\eta} - W_{0,\eta\eta} W_{,\xi\xi} - W_{0,\xi\xi} W_{,\eta\eta}).
\end{aligned} \quad (10)$$

3. BOUNDARY CONDITIONS

Four kinds of boundary conditions along the edges of the panel are studied :

(1) ends simply supported–sides simply supported (BC-1)

$$\begin{aligned} \xi = 0, 1: & \quad F_{,\eta\eta} = \eta_\xi^* \quad F_{,\xi\eta} = -\lambda\eta_{\xi\eta}^* \quad W = 0 \quad M_\xi = 0 \\ \eta = 0, 1: & \quad F_{,\xi\xi} = \lambda^2\eta_\eta^* \quad F_{,\xi\eta} = -\lambda\eta_{\xi\eta}^* \quad W = 0 \quad M_\eta = 0; \end{aligned}$$

(2) sides simply supported–ends clamped (BC-2)

$$\begin{aligned} \xi = 0, 1: & \quad F_{,\eta\eta} = \eta_\xi^* \quad F_{,\xi\eta} = -\lambda\eta_{\xi\eta}^* \quad W = 0 \quad W_{,\xi} = 0 \\ \eta = 0, 1: & \quad F_{,\xi\xi} = \lambda^2\eta_\eta^* \quad F_{,\xi\eta} = -\lambda\eta_{\xi\eta}^* \quad W = 0 \quad M_\eta = 0; \end{aligned} \tag{11}$$

(3) ends clamped–sides clamped (BC-3)

$$\begin{aligned} \xi = 0, 1: & \quad F_{,\eta\eta} = \eta_\xi^* \quad F_{,\xi\eta} = -\lambda\eta_{\xi\eta}^* \quad W = 0 \quad W_{,\xi} = 0 \\ \eta = 0, 1: & \quad F_{,\xi\xi} = \lambda^2\eta_\eta^* \quad F_{,\xi\eta} = -\lambda\eta_{\xi\eta}^* \quad W = 0 \quad W_{,\eta} = 0; \end{aligned}$$

(4) sides clamped–ends simply supported (BC-4)

$$\begin{aligned} \xi = 0, 1: & \quad F_{,\eta\eta} = \eta_\xi^* \quad F_{,\xi\eta} = -\lambda\eta_{\xi\eta}^* \quad W = 0 \quad M_\xi = 0 \\ \eta = 0, 1: & \quad F_{,\xi\xi} = \lambda^2\eta_\eta^* \quad F_{,\xi\eta} = -\lambda\eta_{\xi\eta}^* \quad W = 0 \quad W_{,\eta} = 0, \end{aligned}$$

where η_ξ^* , η_η^* , $\eta_{\xi\eta}^*$ are the nondimensional applied external loads adimensionalized as :

$$\eta_\xi^* = \frac{N_x b^2}{h^2 A_{22}} \quad \eta_\eta^* = \frac{N_y b^2}{h^2 A_{22}} \quad \eta_{\xi\eta}^* = \frac{N_{xy} b^2}{h^2 A_{22}}. \tag{12}$$

To satisfy the boundary conditions the assumed functions are chosen in the following form :

$$F = \eta_\xi^* \eta^2 / 2 + \eta_\eta^* \lambda^2 \xi^2 / 2 - \lambda \eta_{\xi\eta}^* \xi \eta + \sum_{h=1}^m \sum_{k=1}^n F_{hk} X_h(\xi) Y_k(\eta), \tag{13}$$

$$W = \sum_{p=1}^i \sum_{q=1}^j C_{pq} \omega(\xi, \eta), \tag{14}$$

where X and Y are the characteristic clamped-clamped beam functions :

$$X_h(\xi) = \cosh(\varepsilon_h \xi) - \cos(\varepsilon_h \xi) - \alpha_h (\sinh(\varepsilon_h \xi) - \sin(\varepsilon_h \xi)), \tag{15}$$

$$Y_k(\eta) = \cosh(\varepsilon_k \eta) - \cos(\varepsilon_k \eta) - \alpha_k (\sinh(\varepsilon_k \eta) - \sin(\varepsilon_k \eta)). \tag{16}$$

The constants α_h and ε_h are determined with high precision (16 digits) (Zhang and Mathews, 1984) in order to verify the following properties :

$$X_h(0) = X_h(1) = X'_h(0) = X'_h(1) = 0, \tag{17}$$

$$Y_k(0) = Y_k(1) = Y'_k(0) = Y'_k(1) = 0. \tag{18}$$

While the Airy function remains the same, the function $\omega(\xi, \eta)$ is chosen according to the boundary conditions :

- (1) BC-1 $\omega(\xi, \eta) = \sin(h\pi\xi) \sin(k\pi\eta)$
- (2) BC-2 $\omega(\xi, \eta) = X_h(\xi) \sin(k\pi\eta)$
- (3) BC-3 $\omega(\xi, \eta) = X_h(\xi) Y_k(\eta)$
- (4) BC-4 $\omega(\xi, \eta) = \sin(h\pi\xi) Y_k(\eta)$.

4. SOLUTION METHOD

A set of nonlinear algebraic equations (the governing system) in terms of F_{hk} and C_{pq} , unknown coefficients of the approximating series for the Airy function ψ and the out-of-plane function W , and in terms of calculated Galerkin coefficients, has been obtained by using the Galerkin procedure in eqns (9) and (10). The resultant nonlinear algebraic equations in the contracted form are:

$$\sum_m \sum_n C_{mn} D_{mn}^{ij} = \sum_p \sum_q C_{pq} K_{pq}^{ij} + \sum_p \sum_q \sum_r \sum_s C_{pq} F_{rs} G_{pqrs}^{ij} + T(K0^{ij} + \sum_r \sum_s F_{rs} G0_{rs}^{ij}), \quad (19)$$

$$\sum_m \sum_n F_{mn} A_{mn}^{ij} = \sum_p \sum_q \sum_r \sum_s C_{pq} C_{rs} B_{pqrs}^{ij} + T \sum_p \sum_q C_{pq} B0_{pq}^{ij}. \quad (20)$$

The terms A_{mn}^{ij} , B_{pqrs}^{ij} , D_{mn}^{ij} , G_{pqrs}^{ij} and K_{pq}^{ij} concern the situation without initial imperfection T . The terms $B0_{pq}^{ij}$, $G0_{rs}^{ij}$ and $K0^{ij}$ concern the presence of initial imperfection T . These all vary according to various geometric parameters, materials, boundary conditions and Galerkin integrals. The applied loads are contained in the terms K_{pq}^{ij} and $K0^{ij}$. There are two kinds of Galerkin coefficients: second order coefficients such as $\int_0^1 X_h^l X_i d\xi$ in which apex l , up to four, denotes a derivative of that order with respect to the ξ coordinate, and third-order coefficients, such as $\int_0^1 X_h^r X_m^s X_i d\xi$, in which apices r and s denote a derivative with respect to the ξ coordinate. These coefficients also hold true for functions Y_k when replacing ξ with η . While the second order coefficients have been analytically solved (Romeo *et al.*, 1990), the third-order coefficients have been numerically determined using the "ABACI Scientific Desk" software based on the usual integration methods. The POBUCK computer program has been developed to solve the set of nonlinear equations (19) and (20), using an iterative procedure in order to find the postbuckling path at a certain load level. After possible values have been assigned to the unknowns C_{pq} , the first step consists of extracting F_{hk} from eqn (20) and substituting it into eqn (19). The next step is to resolve this final nonlinear system in function of the C_{pq} unknowns and thereby work out the C_{pq} . ABACI software is then employed to resolve the final nonlinear system, using as a base the modified Powell hybrid method for finding the zero of a system of nonlinear functions (Powell, 1970; Abaci, 1987). The user provides a subroutine which calculates the functions and the ABACI code calculates the jacobian by a forward-difference approximation. The iteration is developed until convergence with C_{pq} is reached. The new minimum total potential energy configuration (also with different numbers of half-waves) is obtained starting with the last solution of C_{pq} for subsequent load levels. If convergence has not been reached in this way, one can assign different initial C_{pq} values. The POBUCK software operates on IBM PS2, or higher, requiring about five minutes of CPU, with 36 terms, using the NDP Fortran.

5. ANALYTICAL RESULTS

Several analytical tests have been carried out to prove the accuracy of this procedure by comparing actual results with the few found in literature. The results have been obtained by introducing the initial imperfections as:

$$W_0(\xi, \eta) = T \sin(\pi\xi) \sin(\pi\eta). \quad (21)$$

The correlation with the results found in literature is good, as can be seen by observing Figs 1–4 concerning both the isotropic and anisotropic plate.

In Fig. 1 the Yamaki (1959) results are shown and compared with the present theoretical results for a variously constrained isotropic square plate under uniaxial compression, both with an initial imperfection $T = 0.1$ and without the imperfection. Also reported is the nondimensional out-of-plane deflection, as a function of the nondimensional load. Four kinds of boundary conditions are to be found: I represents a plate with all edges simply supported; II represents sides clamped and ends simply supported; III represents sides simply supported and ends clamped; IV represents a plate clamped along all edges. The

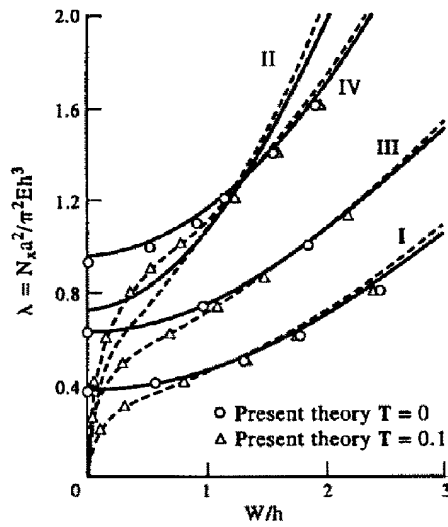


Fig. 1. Load-deflection curves for various boundary conditions isotropic plate under uniaxial compression. Comparison between the present theory and the Yamaki results (Yamaki, 1959).

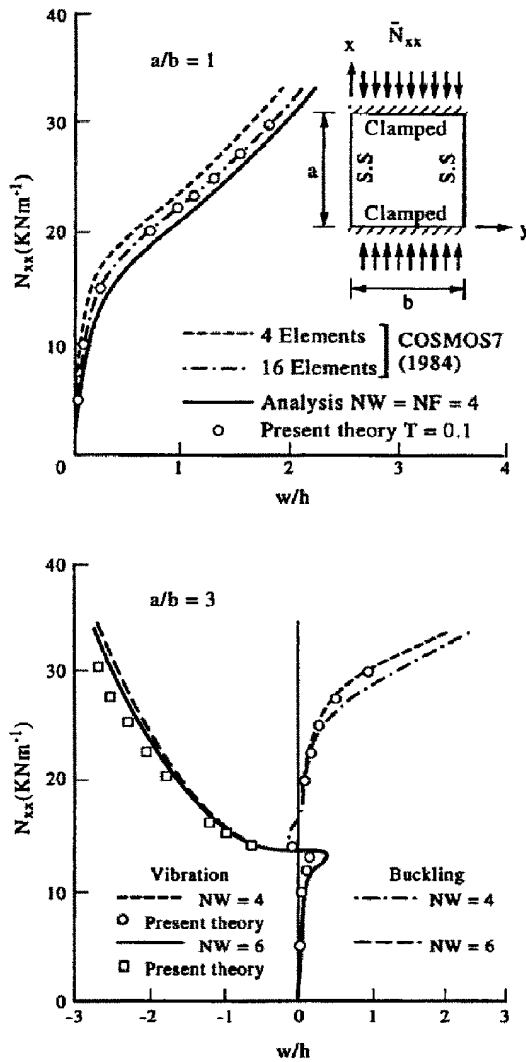


Fig. 2. Load-deflection curves for isotropic plate with various aspect ratios. Comparison between the present theory and the Sheinman results (Sheinman *et al.*, 1991).

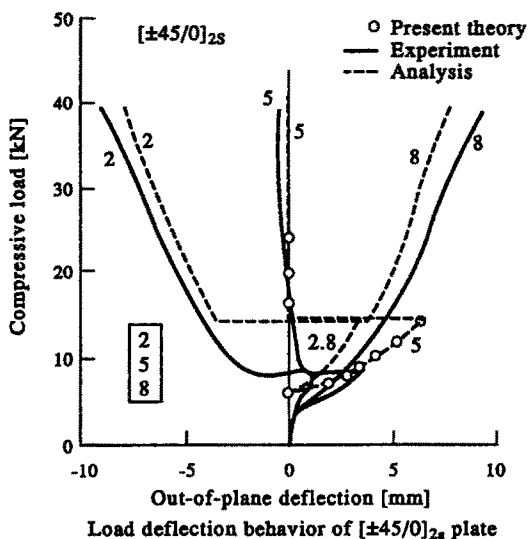
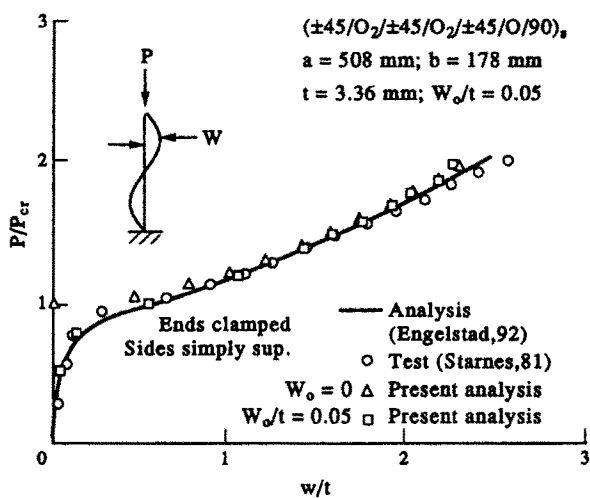
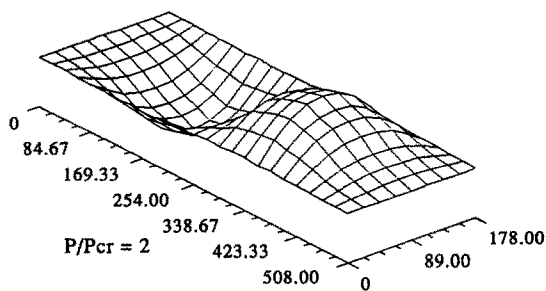


Fig. 3. Load-deflection behaviour for an anisotropic plate under uniaxial compression. Comparison between the present theory and the Minguet results (Minguet *et al.*, 1989).

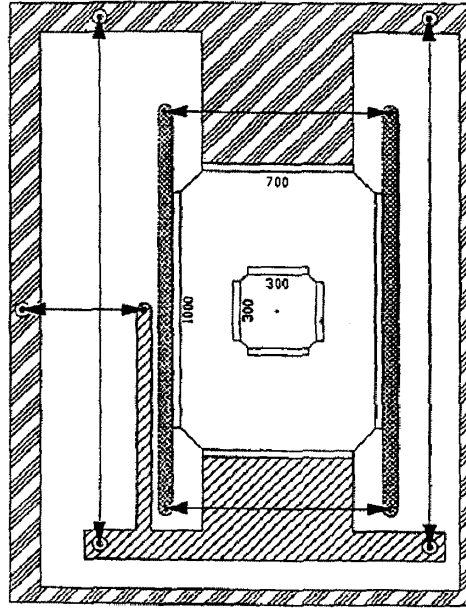
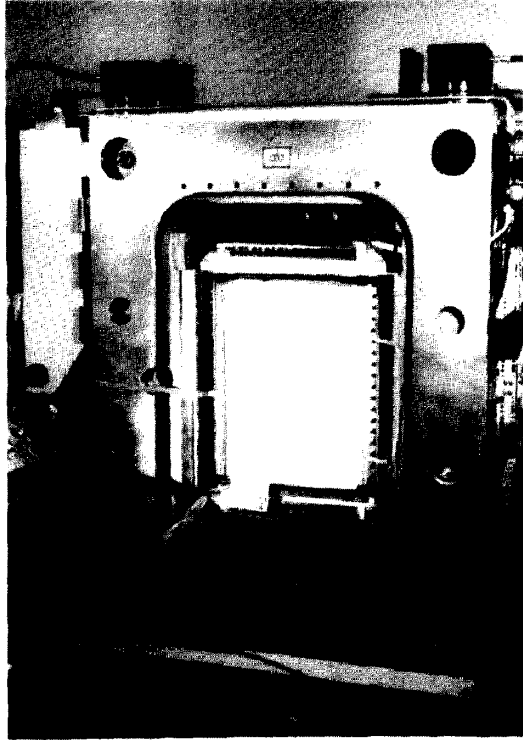





(a)



(b)

Fig. 4. Load-deflection curves of an anisotropic plate under uniaxial compression. Comparison between the present theory and the Engelstad results (Engelstad *et al.*, 1992). (a) Out-of-plane deflection at a quarter length. (b) Overall deflection at $P/P_{cr} = 2$.



-  Longitudinal Loads and Structure
-  Shear Loads and Structure
-  Transverse Loads and Structure

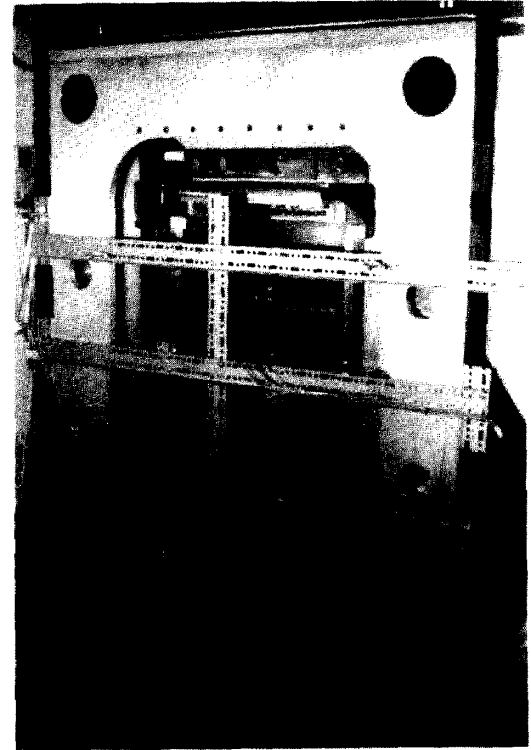
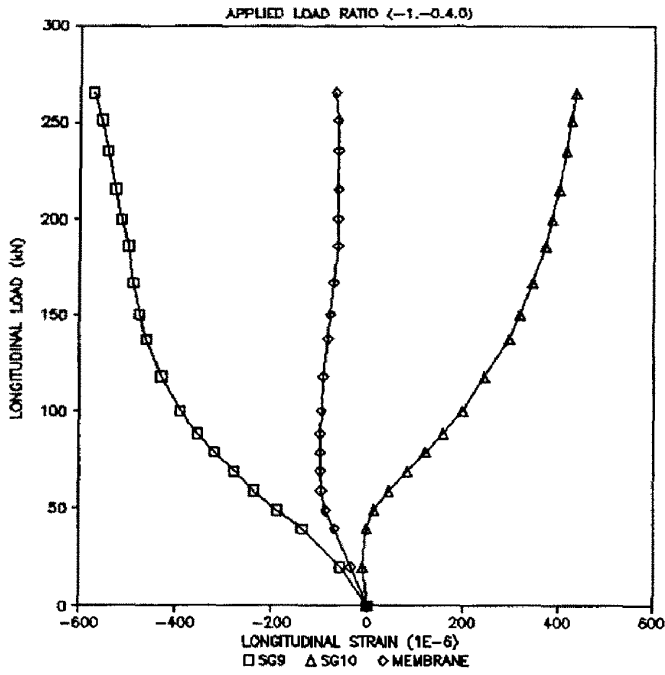
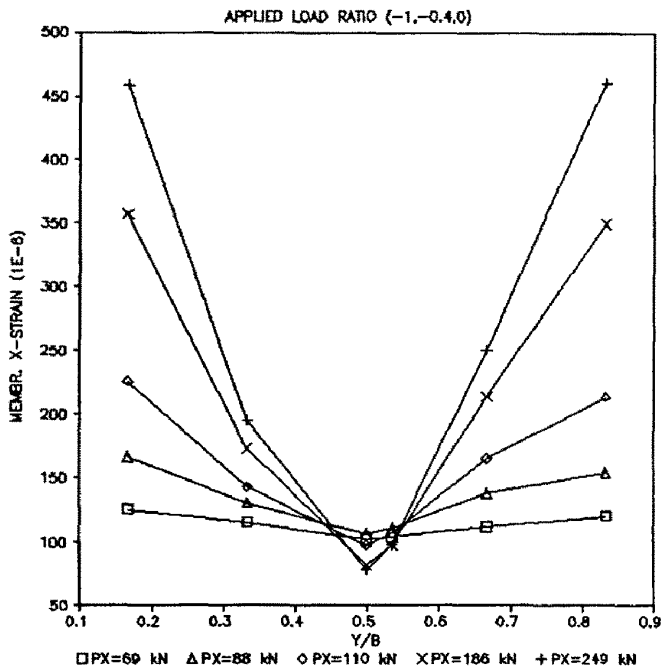


Fig. 5. The new testing machine to apply simultaneously longitudinal compression, transverse compression or tension and positive or negative shear loading.

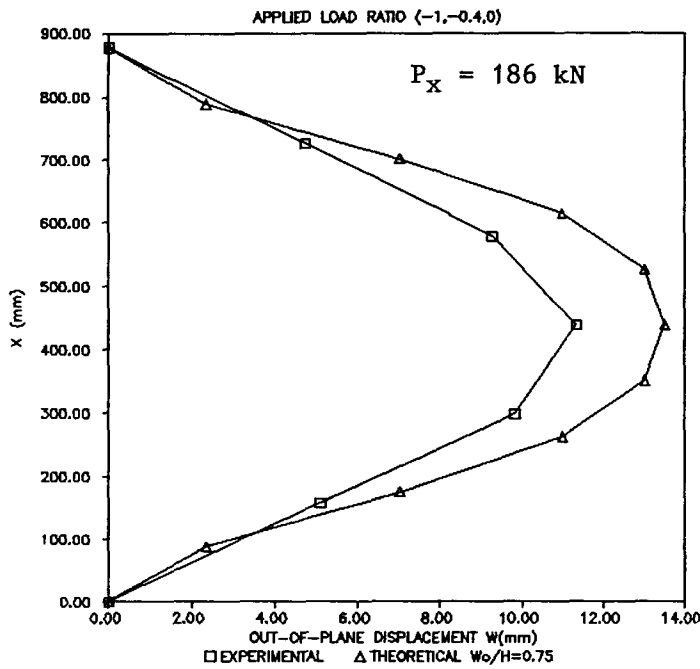
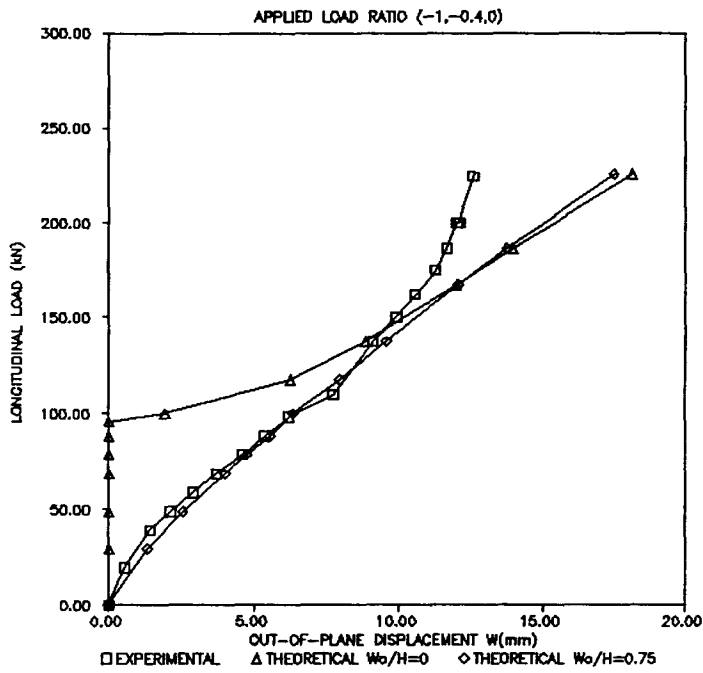


(a)



(b)

Fig. 6. Experimental and analytical results for a clamped anisotropic plate under biaxial compression loading ($N_y = 40\% N_x$). (a) Experimental longitudinal load-strain curves recorded in the centre of the panel. (b) Membrane longitudinal strain distribution across the mid-width for several applied loads.



(c)

Fig. 6(c) Experimental and analytical load-deflection curves at the centre of the panel (above) and across the mid-length (below).

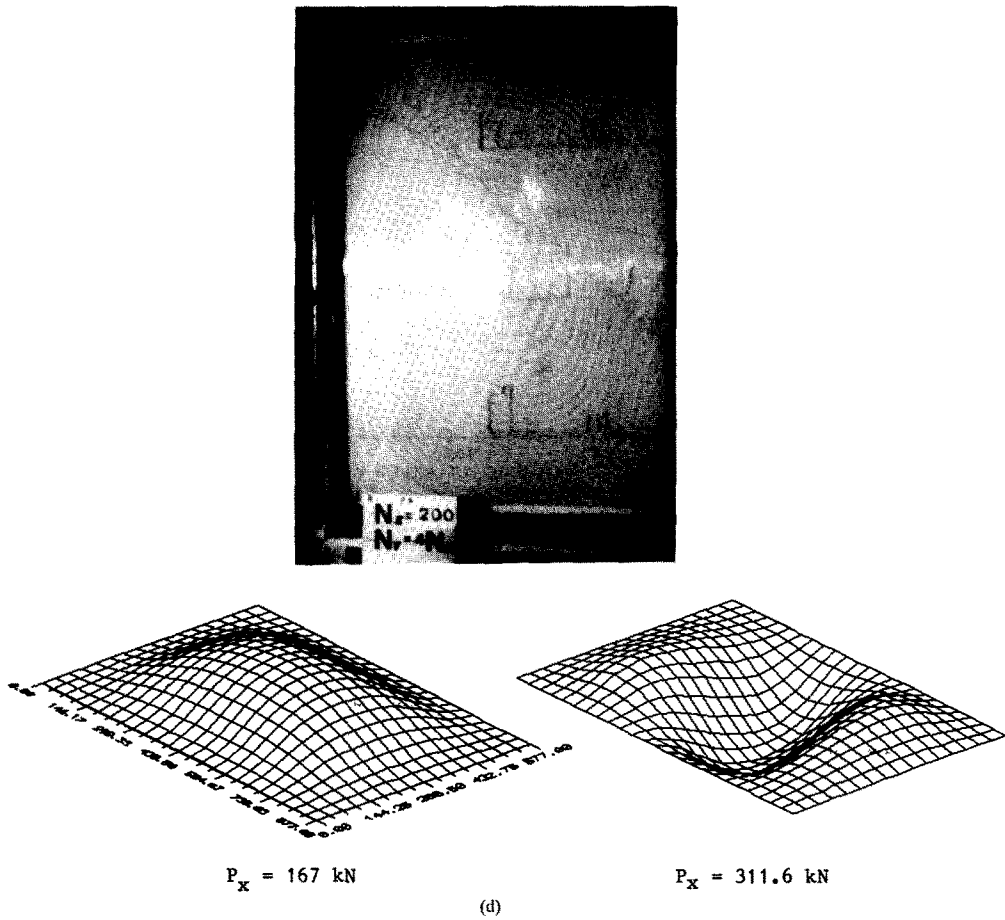


Fig. 6(d) Experimental shadow-Moiré patterns at an applied longitudinal load of 200 kN (above); overall panel deflection theoretical maps at applied loads of 167 and 311.6 kN (below).

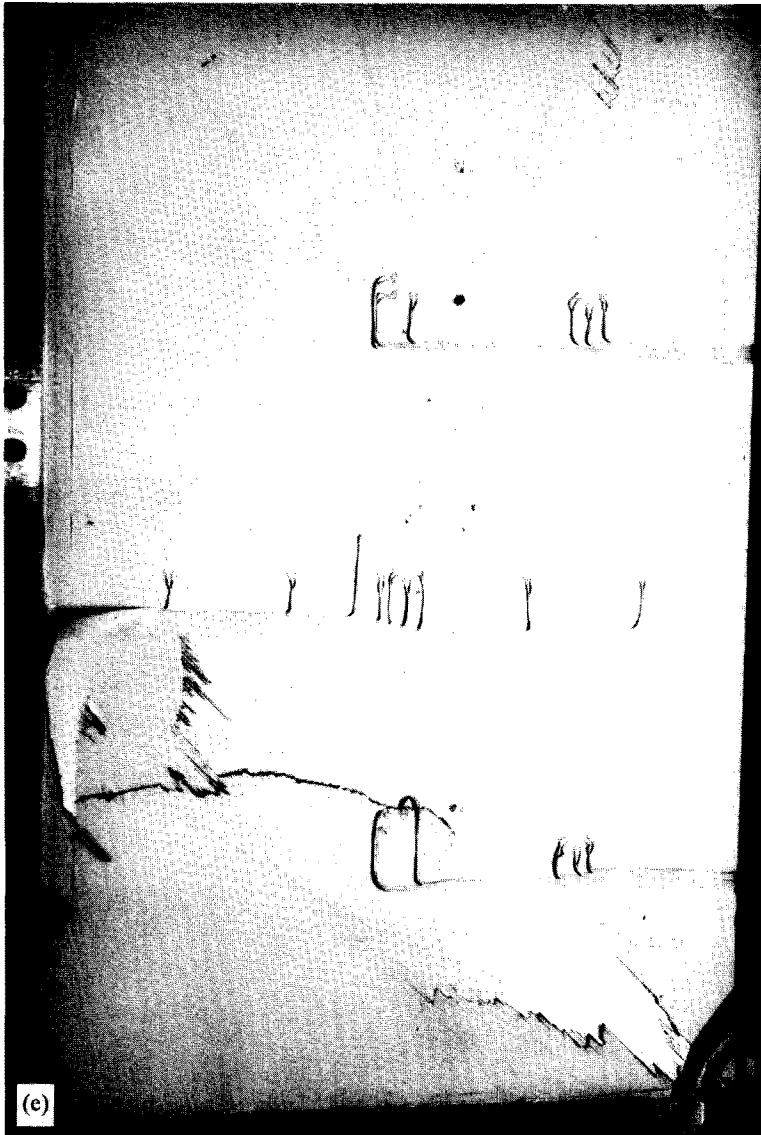
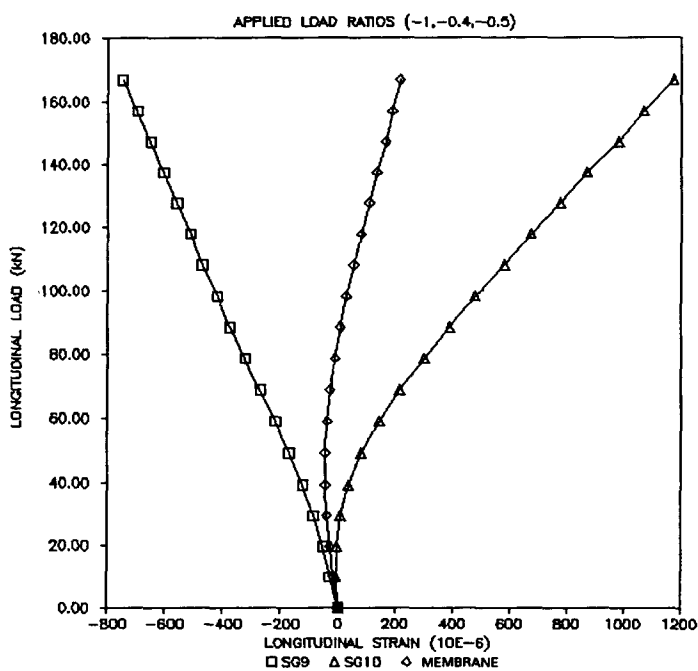
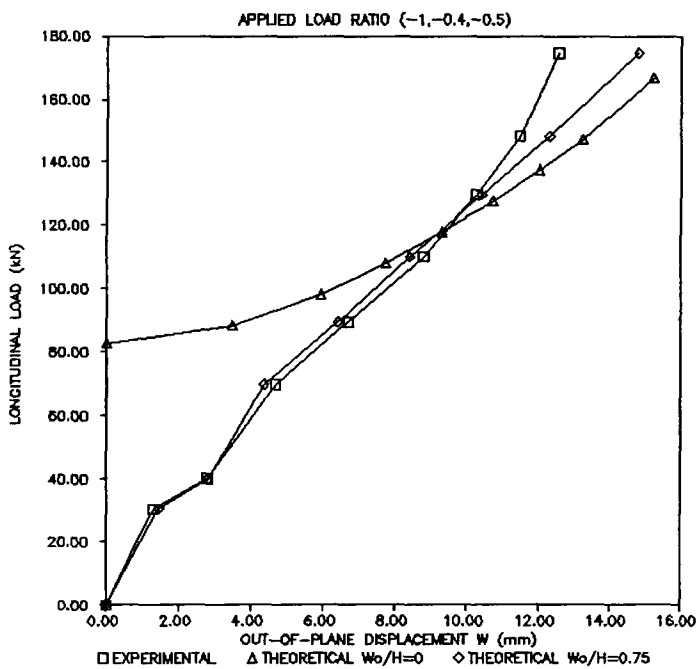


Fig. 6(e) Panel failure.

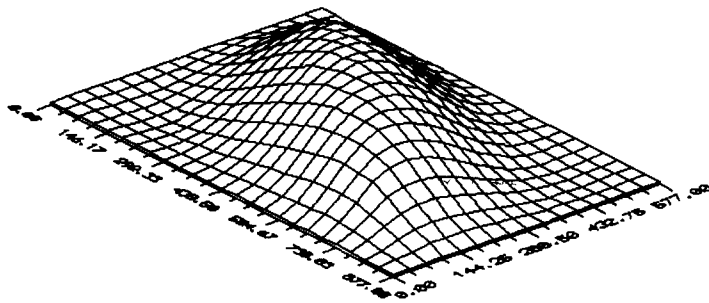
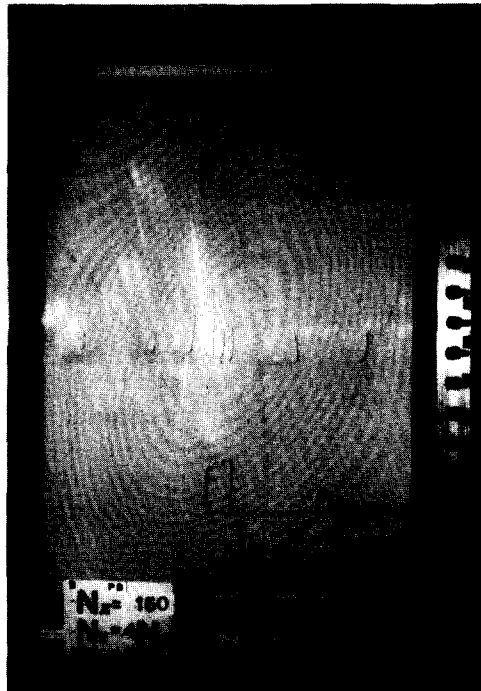


(a)

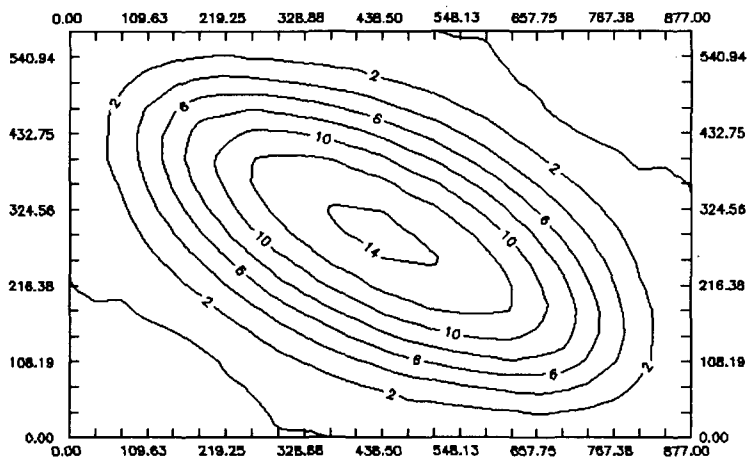


(b)

Fig. 7. Experimental and analytical results for a clamped anisotropic plate under biaxial compression and negative shear loading ($N_y = 40\% N_x$; $N_{xy} = -50\% N_x$). (a) Experimental longitudinal load-strain curves recorded in the centre of the panel. (b) Experimental and analytical load-deflection curves at the centre of the panel.

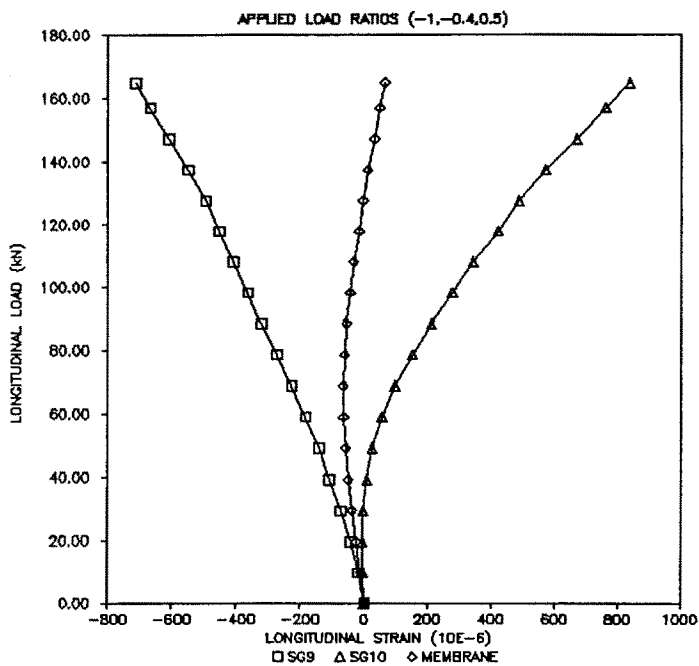


$$P_x = 174 \text{ kN}$$

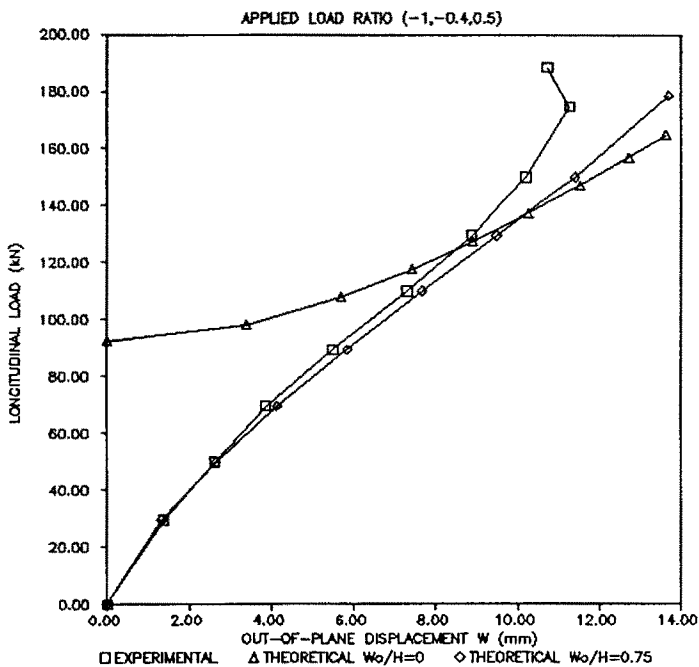


(c)

Fig. 7(c) Experimental shadow-Moiré patterns at an applied longitudinal load of 150 kN (above); overall panel deflection theoretical maps at an applied load of 174 kN (centre and below).

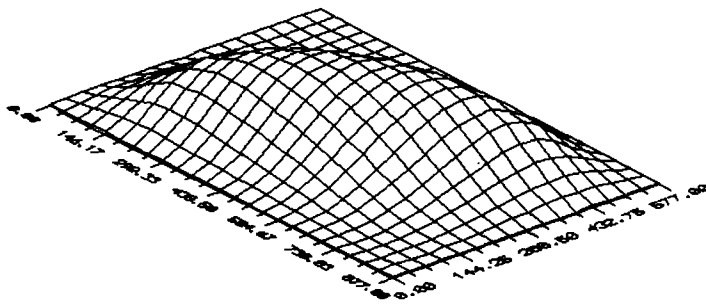
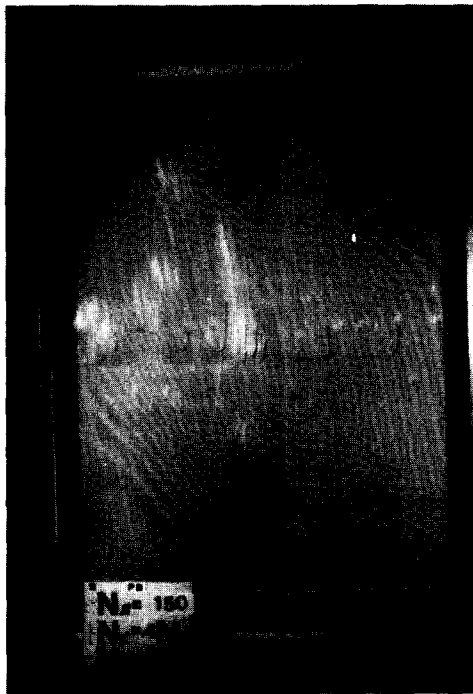


(a)

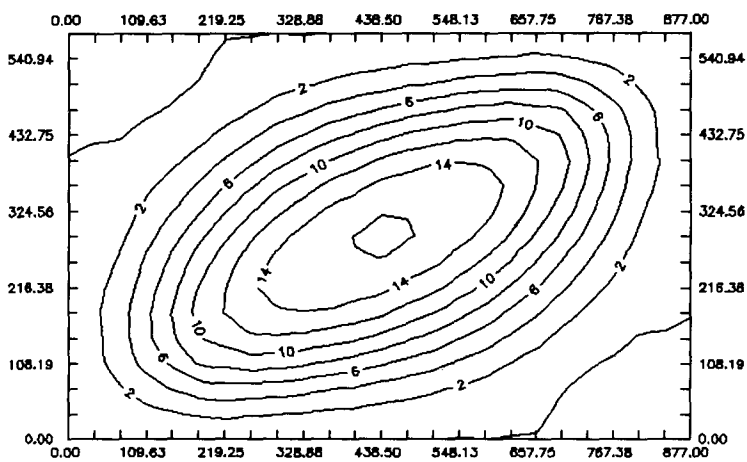


(b)

Fig. 8. Experimental and analytical results for a clamped anisotropic plate under biaxial compression and positive shear loading ($N_y = 40\% N_x$; $N_{xy} = 50\% N_x$). (a) Experimental longitudinal load-strain curves recorded in the centre of the panel. (b) Experimental and analytical load-deflection curves at the centre of the panel.



$P_x = 208 \text{ kN}$



(c)

Fig. 8(c) Experimental shadow-Moiré patterns at an applied longitudinal load of 150 kN (above); overall panel deflection theoretical maps at an applied load of 208 kN (below).

results obtained by the present theory are very close to those of Yamaki. (Note: the results concerning case II are not shown because they refer to another type of initial imperfection.) It can be seen from these results that the postbuckling behaviour of isotropic panels with initial imperfection follows the behaviour of panels without imperfection at least for high level of load beyond the critical load.

Figure 2 (Sheinman *et al.*, 1991) shows the clamped, simply supported isotropic plate under uniaxial compression for the plate aspect ratio $a/b = 1$ and $a/b = 3$; results are reported for the number of terms $m = n = i = j = 4$ and 6, with initial imperfection $T = 0.1$. Two different displacement functions, derived from the solution of beam-vibration or column-buckling problems, have been introduced in the Sheinman paper to solve the nonlinear differential equations. For the plate aspect ratio $a/b = 3$, it should be noted that with the highest number of terms the postbuckling behaviour changes completely from that with the lowest number of terms. It should also be noted that with the increase of the plate aspect ratio, the initial imperfections cause a behaviour which is quite different from the theoretical behaviour without the imperfections.

In Fig. 3 (Minguet *et al.*, 1989) the results are reported for an anisotropic square plate under uniaxial compression; the plate has the edges clamped and the sides simply supported. Only the middle out-of-plane displacement (5) is reported in the present paper; the initial imperfections are not included, since data were not reported in the Minguet paper. A very good correlation has been obtained, which includes the transition from the first buckling mode to the second.

Figure 4 (Engelstad *et al.*, 1992) reports a comparison between analytical and experimental results on a rectangular anisotropic plate under uniaxial compression. The plate has clamped edges and simply supported sides and initial imperfection $T = 0.05$. Figure 4a shows the panel deflection obtained with the present theory at a quarter length as a function of the applied load normalized by the analytical buckling load. Figure 4b shows the panel deflection obtained with the present theory at an applied load of $2.0P_{cr}$. The results obtained using the present theory converge very well with the experimental ones (Starnes and Rouse, 1981), as well as with the analytical results obtained in the Engelstad paper by a finite element method and including the transverse shear deformation. From this comparison, it seems that the postbuckling deflection of thin panels is not affected by the transverse shear deformation for loads below failure value.

6. EXPERIMENTAL RESULTS

Since experimental results on panels subjected to biaxial compression and shear loads were not found in literature, a new testing machine has been built by the Italian company "AIP Studio" in order to apply simultaneously the above combined loads (Fig. 5). A maximum longitudinal compression load of 490 kN, a transverse compression or tension load of 196 kN and a positive or negative shear load of 196 kN can be applied to panels with dimensions smaller than 1000 by 700 mm. Longitudinal load is applied by two separately controlled servo-actuators; a displacement control is used to keep the panel ends parallel to each other, their angular rotation controlled to zero with an accuracy of 0.001° . The transverse load application system, which is made up of two separately controlled servo-actuators, floats in order not to interfere with the longitudinal and shear loads. Shear load is applied to the bottom end of the panel by a servo-actuator. The test rig is completely loop-controlled via electronic modules which are closed by nine transducers (Romeo and Frulla, 1992).

Experimental and analytical results have been obtained relative to an anisotropic panel with a symmetric lay up $(-45/0_4/45/90)_{3s}$, in which $a = 877$ mm, $b = 577$ mm and $h = 5.52$ mm; the panel was manufactured in a graphite/epoxy material and was vacuum bagged and autoclave cured. The material properties used for the computations are:

$$E_1 = 209.3 \text{ GPa}; \quad E_2 = 6.89 \text{ GPa}; \quad G_{12} = 4.26 \text{ GPa}; \quad \nu_{12} = 0.305.$$

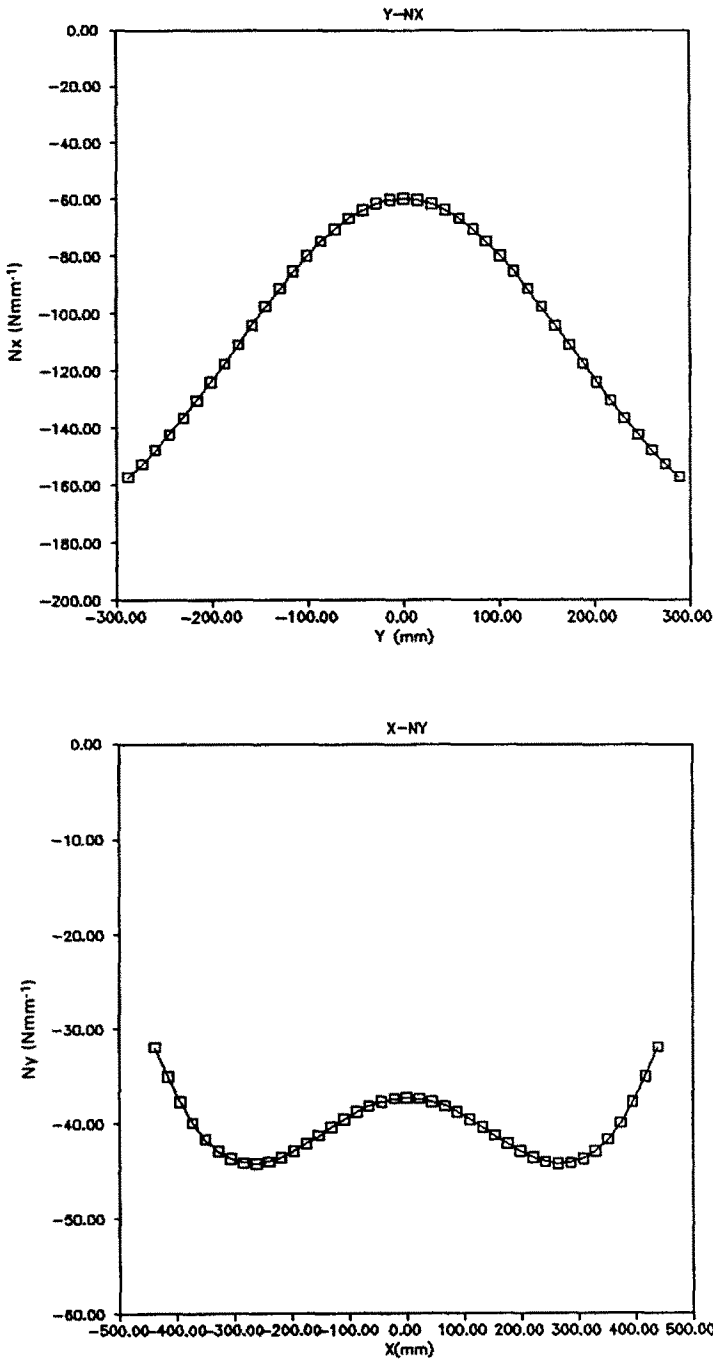


Fig. 9. Load, per unit width, distribution across the ends (above) and across the sides (below) for a simply supported anisotropic panel under biaxial compression ($N_{x_{av}} = 100 \text{ N mm}^{-1}$; $N_{y_{av}} = 40 \text{ N mm}^{-1}$).

An initial imperfection, referring to the middle surface, was measured close to the assumed $W_0(\xi, \eta)$ function when the value of T is 0.75. The panel boundary conditions assumed all edges to be clamped, although there were some difficulties in the carrying out of the experimental clamping. A series of tests were sequentially carried out: a pure biaxial compression test with load per unit width ratio of $(-1, -0.4, 0)$, with respect to the longitudinal load, a combined biaxial compression and negative shear test with load ratio of $(-1, -0.4, -0.5)$ and another combined biaxial compression and positive shear test with load ratio of $(-1, -0.4, 0.5)$.

Table 1. Analytical and experimental results for clamped panel under combined biaxial compression and shear load

Applied load ratio			Buckling load per unit width (N mm ⁻¹)						
			Analytical Present theory			Experimental Membrane strain constant			Southwell method
N_x/N_x	N_y/N_x	N_{xy}/N_x	N_x	N_y	N_{xy}	N_x	N_y	N_{xy}	N_x
-1	0	0	-297	0	0	-285	0	0	-305
-1	-0.4	0	-166	-66	0	-153	-61	0	-164
-1	-0.4	+0.5	-160	-64	+80	-145	-58	+73	-153
-1	-0.4	-0.5	-143	-57	-71	-125	-50	-63	-148

The out-of-plane displacement was measured using 10 computer-controlled magnetic-resistive transducers positioned on the centre cross-lines of the panel. A qualitative representation of the out-of-plane deflection was obtained, simultaneously to the transducer acquisition, with the shadow-Moiré method.

A summary of the buckling results is reported in Table 1, including the theoretical buckling load per unit width obtained by the present analysis. The experimental critical load at which the panel displayed buckling was defined by the load vs strain curves as the value at which the membrane strain does not increase further. Results are also reported for the buckling loads obtained from the experimental load-deflection curves using the Southwell method.

Experimental and analytical results are reported in Fig. 6 for the panel under biaxial compression; transverse load is 40% of the longitudinal load. The applied load is first reported (Fig. 6a) as a function of two back-to-back strain gauges placed at mid-length and mid-width; the measured surface strains were not uniform with the load from the start because of the presence of an initial imperfection. After buckling, there was no further increase in the membrane strain at half-width, at half-length and quarter-length from the bottom and top edges; however, strain gauges placed near the sides still registered an increase in the membrane value. The strain distribution over the entire cross panel mid-width is shown in Fig. 6b for five values of the applied load; the y coordinate across the panel is normalized by the panel width b .

The out-of-plane central deflection is then reported (Fig. 6c) as a function of the applied longitudinal load; as expected, the presence of an initial imperfection meant that the transverse displacement increased with the load from the start. The authors' analytical results, obtained with 16 terms, are in very good correlation with the experimental data up to 1.5 times the critical load. In the authors' opinion, this is due to the fact that the panel behaviour passes from one half-wave to two or more half-waves during load increase, assuming an alternative equilibrium configuration. Different configurations, beyond a certain load level, were obtained by the authors through the present theory. The overall panel deflection analytical maps are represented in Fig. 6d; they refer to an applied load of 167 kN (one half-wave) and 311.6 kN (three half-waves).

After carrying out the tests under combined biaxial compression and shear, a second experimental test of biaxial compression was carried out up to failure load. The panel failed catastrophically at a longitudinal load of 285 kN; visually it appeared that the number of buckling half-waves changed just before failure occurred; however, it was not possible to record any experimental data in time. As can be seen from the panel failure represented in Fig. 6e, damage occurred not only near edges and supports but also along a nodal line placed at about one-third of the panel length. Even though transverse stresses should significantly contribute to failure initiation, transverse shear deformation has not been considered to date in the postbuckling path.

Experimental and analytical results obtained for the panel under biaxial compression and negative or positive load are reported in Figs 7 and 8; the transverse and shear loads are respectively 40% and 50% of the longitudinal load. The same behaviour was recorded as for the former tests, but for different loads. The effects of the shear load on the panel

behaviour are not so high with respect to the biaxial compression ; this is mainly due to the panel lay-up.

7. CONCLUSIONS

Results reported here permit the following conclusions :

(a) The POBUCK computer program is well structured and gives results consistent with those found in literature and with the experimental results obtained.

(b) Extended testing activity is necessary to investigate other boundary conditions and to verify the behaviour for much higher loads.

(c) The existence of different equilibrium configurations for certain loads requires the development of another computer procedure to verify that the previously calculated equilibrium situations are in fact minimum conditions for total potential energy.

(d) A second reason for the difference between the analytical and experimental out-of-plane deflection recorded at loads much higher than the critical load is due to the boundary conditions on the sides of the panel. Both sides and ends, in fact, are constrained to remain straight by the steel clamps of the machine ; for example, in a panel under uniaxial compression, tensile stresses are developed in the transverse direction on the centre portion, reducing the out-of-plane deflection (Timoshenko and Gere, 1961). A new theoretical analysis is in progress to take into account this effect. A simply supported anisotropic plate under biaxial compression has been considered up to the moment ; the components u and v of the displacements are kept constant along the four sides of the panel. By applying the principle of the stationary value of the total potential energy a solution has been obtained and the results are reported in Fig. 9. The plate investigated has the same lay-up of the panel tested under biaxial compression ; transverse load is 40% of the longitudinal load. The load along the width, N_x , and along the length, N_y , is reported at an applied average longitudinal load of 100 N mm^{-1} ; as it is very clear, in the post-buckling field, the distribution of the compressive load is no longer uniform along the sides ; in particular, the larger portion of the longitudinal load is taken by the portion of the plate near the edges, while for the transverse load a lower value is applied on the centre portion with respect to the average applied load. As consequence, a lower out-of-plane deflection will result. The solution for the clamped plate is under development.

Further efforts might be directed to the examination of these problems with the purpose of improving the correlation between theoretical and experimental data.

REFERENCES

- Abaci, C. (1987). *The Scientific Desk—User Guide*. Abaci.
- Chia, C. Y. (1980). *Nonlinear Analysis of Plates*. McGraw-Hill, New York.
- Engelstad, S. P., Reddy, J. N. and Knight, N. F. Jr. (1992). Postbuckling response and failure predictions of graphite–epoxy plates loaded in compression. *AIAA J.* **30**(8), 2106–2113.
- Minguet, P. J., Dugundji, J. and Lagace, P. (1989). Postbuckling behaviour of laminated plates using a direct energy minimization technique. *AIAA J.* **27**(12), 1785–1792.
- Powell, M. J. D. (1970). A hybrid method for nonlinear equations. In *Numerical Methods for Nonlinear Algebraic Equations* (Edited by P. Rabinowitz). Gordon and Breach.
- Romeo, G., Alonso, C. and Pennavaria, A. (1990). Buckling of laminated cylindrical plates including effects of shear deformation. In *Proceedings International Symposium on Space Application of Advanced Structural Materials*, ESA SP-303, 365–370. Noordwijk, The Netherlands.
- Romeo, G. and Frulla, G. (1992). Postbuckling behaviour of anisotropic plates under biaxial compression and shear loads. In *ICAS 1992, Proceedings of the 18th Congress of the International Council of the Aeronautical Sciences*, Vol. II, pp. 1936–1944. Beijing, P.R. China.
- Rouse, M. (1985). Postbuckling of flat unstiffened graphite epoxy plates loaded in shear. In *Proceedings of the AIAA/ASME/ASCE/AHS 26th SDM Conference*, pp. 605–616. Orlando, Florida.
- Sheinman, I., Frostig, Y. and Segal, A. (1991). Nonlinear analysis of stiffened laminated panels with various boundary conditions. *J. Compos. Mater.* **25**, 634–649.
- Starnes, J. H., Dickson, J. N. and Rouse, M. (1984). Postbuckling behaviour of graphite–epoxy panels. In *Proceedings ACEE Composite Structures Technology*, NASA CP-2321, pp. 137–159. Seattle, Washington.
- Starnes, J. H. and Rouse, M. (1981). Postbuckling and failure characteristics of selected flat rectangular graphite–epoxy plates loaded in compression. *AIAA Paper* 81-0543.

- Stein, M. (1985). Postbuckling of long orthotropic plates under combined loading. *AIAA J.* **23**(8), 1267–1272.
- Timoshenko, S. P. and Gere, J. M. (1961). *Theory of Elastic Stability*, 2nd edn. McGraw-Hill, New York.
- Yamaki, N. (1959). Postbuckling behaviour of rectangular plates with small initial curvature loaded in edge compression. *J. appl. Mech.* **26**, 407–414.
- Zhang, Y. and Matthews, F. L. (1984). Postbuckling behaviour of anisotropic laminated plates under pure shear and shear combined with compressive loading, *AIAA J.* **22**(2), 281–286.
- Zhang, Y. and Matthews, F. L. (1985). Large deflection behaviour of simply supported laminated panels under in-plane loading. *J. appl. Mech.* **52**, 553–558.